Available online at www.sciencedirect.com
SCIENCE DIRECT®
Ultrasonics 42 (2004) 205–212
Ultrasonics
www.elsevier.com/locate/ultras

Optimisation using measured Green's function for improving spatial coherence in acoustic measurements

Matthew Clark *, Steve D. Sharples, Mike Somekh

Applied Optics, Electrical and Electronic Engineering, University of Nottingham, University Park, Nottingham NG7 2RD, UK

Abstract

Aberrating materials can degrade acoustic measurements by distorting the acoustic wavefront and causing acoustic speckle (as opposed to speckle noise which is a manifestation of coherent backscatter). The amplitude and phase fluctuations associated with acoustic speckle can introduce considerable measurement uncertainty which is difficult to deal with.

This paper demonstrates a new technique which optimises the spatial distribution of the generation of the ultrasound to compensate for the aberration. This technique uses experimentally measured Green's functions to allow the calculation of the field resulting from the generation wavefront during optimisation.

The technique is used to improve the accuracy of velocity measurements in a steel sample using 82 MHz SAW waves. This is achieved by optimising for improved spatial coherence in the measurement region which suppresses the speckle noise.

Experimental evidence of acoustic aberration arising from grain structure is shown for steel and aluminium and the measured Green's function optimisation technique is shown to overcome the resulting acoustic speckle. The technique was performed using the Adaptive Optical Scanning Acoustic Microscope (AOSAM) at Nottingham University, UK.
© 2004 Elsevier B.V. All rights reserved.

Keywords: Acoustic aberrations; Stochastic media; Scattering; Optimisation; Velocity measurement

1. Introduction

Acoustic aberrations or distortions of the acoustic wavefront can arise from acoustic velocity variations in the medium in which the acoustic wave propagates. Acoustic velocity variations can be caused by a range of factors: the most common in metals is the presence of microstructure or grains. Most metals are polycrystalline being made up of randomly distributed grains.

In this paper experimental evidence for the existence of aberrating microstructure in metals is presented using a novel instrument—an optical scanning acoustic microscope (OSAM [1,2]) at 82 MHz with surface acoustic waves (SAWs). The experimental evidence is backed up by simulation results showing that the spatial coherence can be projected away from the source.

The OSAM is used to measure the Green's function response of the sample, and then this Green's function is used to optimise the generation of the SAWs, producing a region of extended spatial coherence which would normally be destroyed by the acoustic aberrations. The spatially coherent region can then be used to perform acoustic measurements with greater certainty than is otherwise possible.

In this paper this technique is used to produce an area of high spatial coherence away from the SAW source and thus overcome the limitations imposed by the aberrations. This area of high spatial coherence is then used to perform a high quality velocity measurement. While it is possible to produce an estimate of the velocity from the measured Green's functions themselves the main purpose of this paper is to demonstrate that spatial coherence can be restored to the measurement region (and projected away from the source) despite the aberrating microstructure.

1.1. Acoustic aberrations

Fig. 1 shows SAW propagation on a homogeneous (glass) sample. The image was taken using an OSAM by generating a plane SAW and scanning the detector to build up an image of the propagating wave. The wave propagates from left to right and just diffracts slightly,

* Corresponding author. Fax: +44-115-9515616.
E-mail address: matt.clark@nottingham.ac.uk (M. Clark).

0041-624X/$ - see front matter © 2004 Elsevier B.V. All rights reserved.
doi:10.1016/j.ultras.2004.01.009

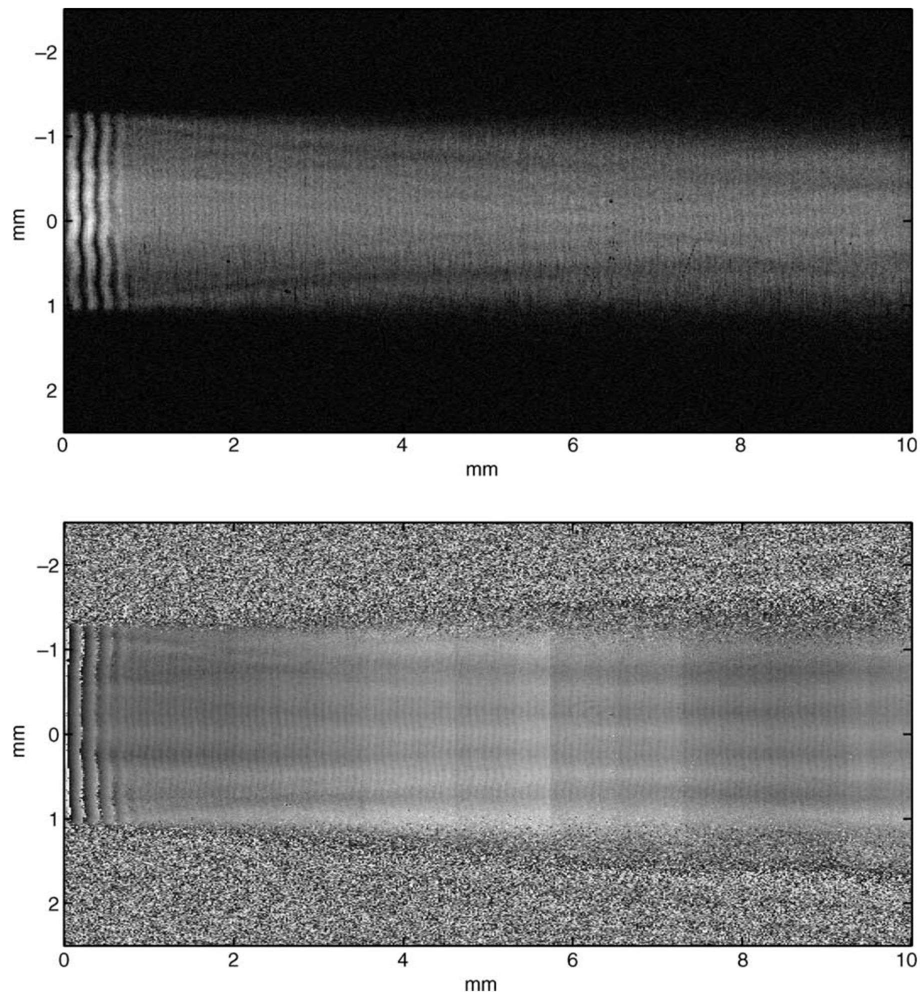

Fig. 1. 82 MHz SAW propagation on a homogeneous sample (glass) (upper amplitude, lower residual phase). The beam propagates perfectly in this homogeneous sample just diffracting slightly over this distance. Residual phase is the phase distribution with the zero-order phase of propagation removed leaving the relative spatial variation.

experiencing no aberration and little attenuation. Figs. 2 and 3 show similar experiments on aluminium and steel respectively. In marked contrast to the image on glass (Fig. 1) they are dominated by acoustic speckle. The speckle in the amplitude distribution is accompanied by large fluctuations in the SAW phase. The speckle can be shown to result from the materials microstructure which causes aberration of the acoustic wavefront, which can be thought of as separate from scattering [3]. The aberration is caused by different parts of the wave experiencing different acoustic velocities resulting in distortion of the wavefront and speckle.

The acoustic speckle has a negative effect on measurement quality. This paper concentrates on a particular measurement, acoustic velocity, however the effects are more general (in particular the probability of detection of defects can be reduced by aberrations because of the chance of missing the defect with ultrasound).

Velocity measurements are usually made by measuring the acoustic phase a two points or more points and inferring the phase gradient. It is possible to obtain extremely accurate velocity measurement with this technique in isotropic samples [4] or single crystal anisotropic samples. However, in aberrating media the aberrations and associated speckle can significantly increase the measurement error. There are three main effects: (1) the amplitude variations can mean that there is not enough signal at one or more of the measurement points, (2) the local phase gradient is distorted and (3) the measurement points occur on different speckles which may have decorrelated phase distributions.

The signal loss caused by aberrations can far exceed that caused by scattering (or attenuation). Fig. 4 shows the acoustic power distribution of the image shown in Fig. 3. This also shows the transverse integral of the power distribution which is a measure of the total acoustic power with distance. This shows that the vari-

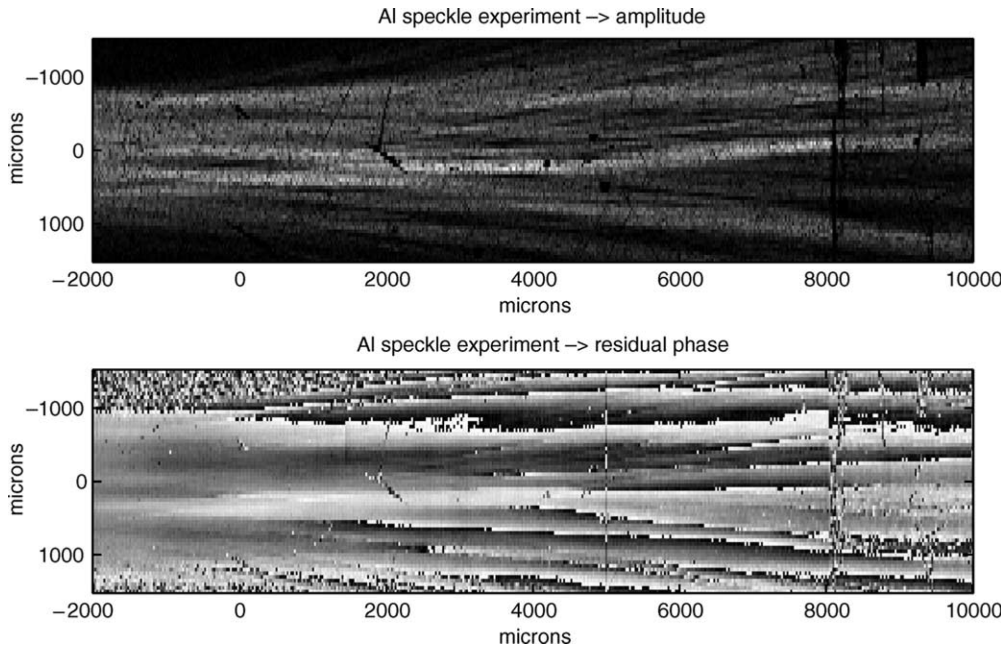

Fig. 2. 82 MHz SAW propagation on an aluminium sample (upper amplitude, lower residual phase). The amplitude is broken up into acoustic speckles as it propagates from left to right. The pattern of speckles is random and determined by the exact position of the sample. The statistical properties of the speckles (e.g. size, strength of variation etc.) can be related to the statistical properties of the randomly varying medium (grain structure). The variations in amplitude are accompanied by large variations in the phase.

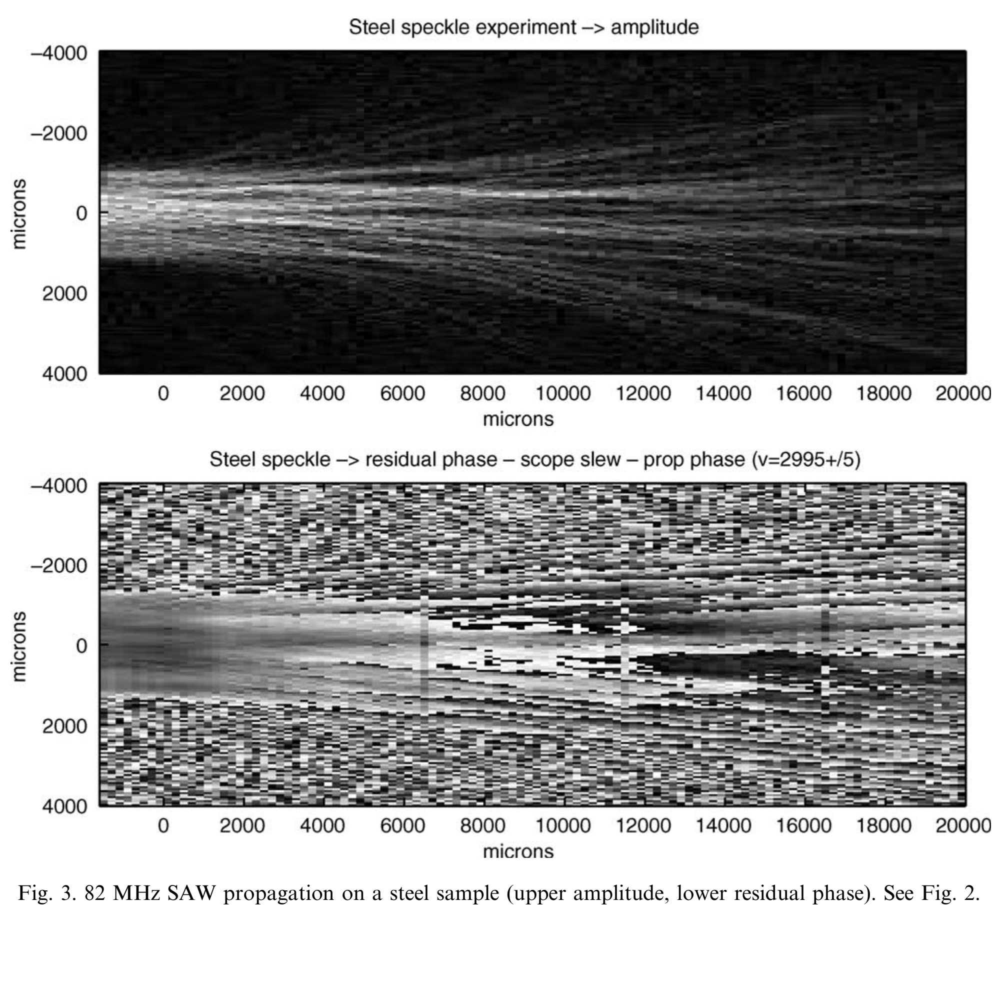

Fig. 3. 82 MHz SAW propagation on a steel sample (upper amplitude, lower residual phase). See Fig. 2.

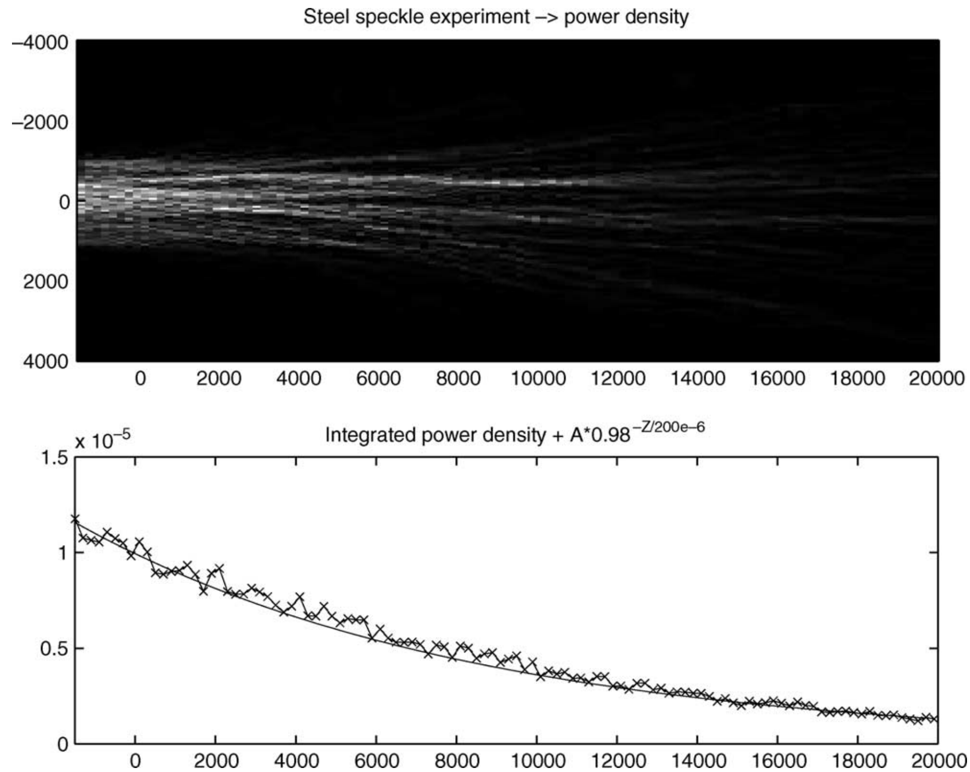

Fig. 4. Acoustic power density on steel (upper) and power vs propagation distance (lower). The solid line is a fit based on a simple scattering loss model based on an estimate of the power lost through reflections at grain boundaries.

ations in amplitude caused by acoustic aberrations can be far more significant than the losses caused by scattering.

1.2. Adaption

We have previously shown that it is possible to adapt the initial wavefront of the acoustic source to compensate for aberrations [5] using an adaptive source [6]. However this work was based on a focused beam. The phase change associated with going through a focus means that the use of a focused patch of ultrasound to measure the phase gradient is subject to error (because the size of the focus is affected by the aberrations) and that these techniques alone are not suitable for dealing with this problem.

1.3. Time reversal

Time reversal techniques fail to improve the spatial coherence for this experimental case. Both simulation and experiment have shown that the information loss is too great for a time reversed signal to converge. This results from the experimental "open cavity" [7], from attenuation and scattering loss and from the finite aperture size of the source. This can be understood be examining Figs. 2–4. The reversal must come from the limited spatial aperture afforded by the experiment (in this case the spatial light modulator (SLM) [6]). This limited aperture cannot reverse the parts of the wavefront that lie beyond it, which amounts to information loss. In this case the limited aperture time reversed signal is worse than the original flat wavefront.

1.4. Optimisation

In this paper we present a new technique which is based on improving the spatial coherence of the wave at the measurement zone rather than just correcting the aberration. This uses measured Green's functions and an optimisation algorithm to improve the spatial coherence where adaption or time reversal would fail.

2. Optimisation using measured Green's functions

In this technique we use a direct-search optimisation method (originally developed for the design of computer generated holograms [8]) to optimise the generation wavefront to compensate for the acoustic aberrations. There are two main differences between [8] and this new technique: (1) the Green's function $G(R,S)$, of the system cannot be determined analytically because of the stochastic nature of the media and therefore must be

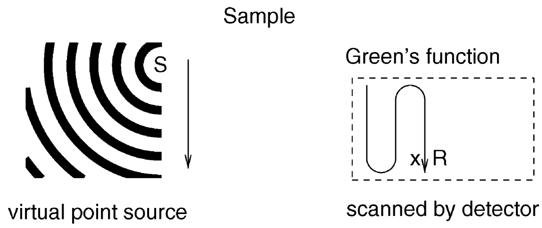

Fig. 5. Schematic of the experimental system, the pseudo point source at S and the point detector at R are scanned to build up $G(R,S)$.

determined experimentally and (2) the target for the optimisation is applied to the amplitude and phase of the acoustic wave in the measurement zone with the aim of increasing the spatial coherence.

2.1. Measuring $G(R,S)$

In a stochastic medium the deterministic Green's function, $G(R,S)$, is a function of source, S and receiver, R position. It can be determined by generating a wave with a point source at S and receiving it with a point receiver at R. Experimentally it is measured in the OSAM using a pseudo point source and true point receiver. The source and receiver positions are then scanned to build up $G(R,S)$ (see Fig. 5).

2.2. Optimisation

The optimisation of the source is performed as in [8] using $G(R,S)$ and a cost function of the form $C = -a|\bar{U}| + b\sigma|U| + c|\bar{U}|\arg(U)$, where U is the complex amplitude of the wave evaluated over the region of interest as $U(R) = \int G(R,S)e^{-i\phi_d}\,dS$, σ denotes standard deviation, arg the phase, ϕ_d the design phase and a, b and c are cost balancing factors specific to the problem [8]. $|\bar{U}|$ appears in the third term of C as a scaling factor that prevents one term dominating the design.

3. Results

3.1. Simulation and spatial coherence

The effect on the spatial coherence of the wave has been investigated using a simulation model. The model is based on a phase screen approximation [9] and uses a simulated medium based on the random growth of grains. We have used the transverse autocorrelation function of the wave as a measure of spatial coherence. Figs. 6 and 7 show a typical simulation result. It can be seen that in the case of a plane wavefront the spatial coherence has decayed between the source and detector, and in the case of the optimised wavefront the spatial coherence is initially low and builds to a maximum at the measurement zone.

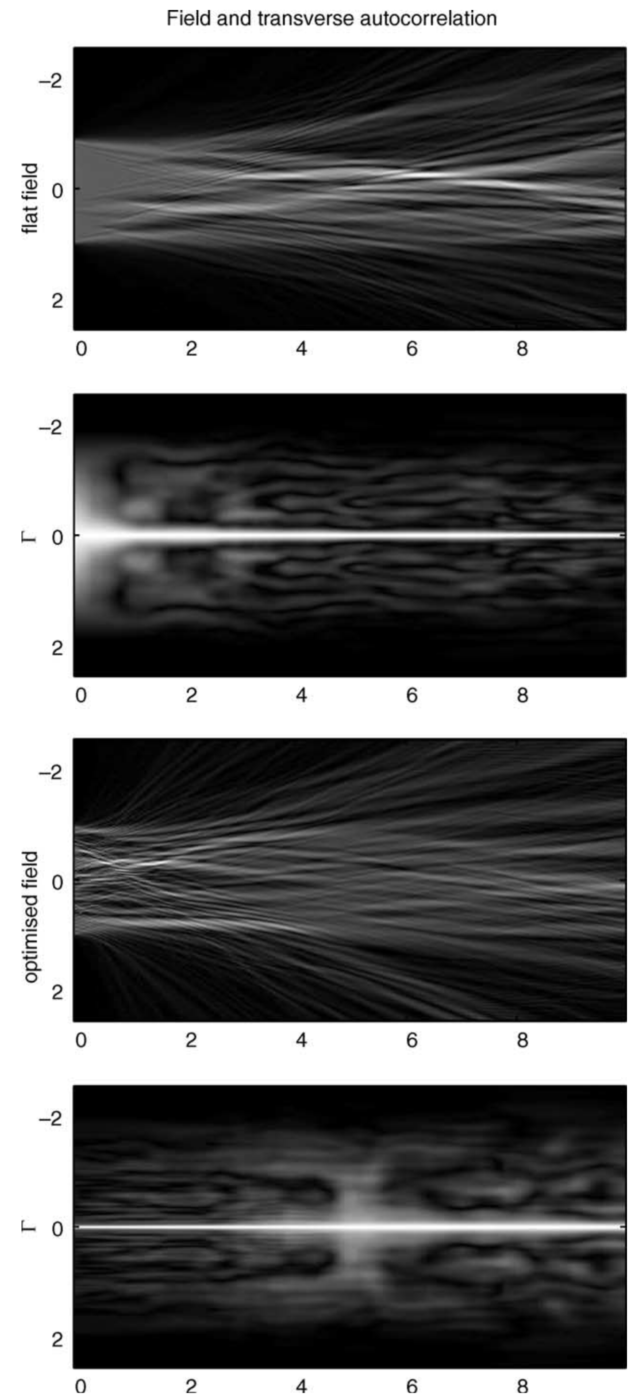

Fig. 6. Simulation of experiment showing increased spatial coherence at the measurement zone in the case of optimisation (82 MHz SAWs/ "large" grains/scale in mm). The target region for the optimisation was an aperture the size of the source located at a distance of 5 mm from the source.

3.2. Experiment and measurement error

Fig. 8 shows a part of a measured Green's function taken on a piece of steel corresponding to a range of S and R taken using an OSAM with 82 MHz SAWs. The

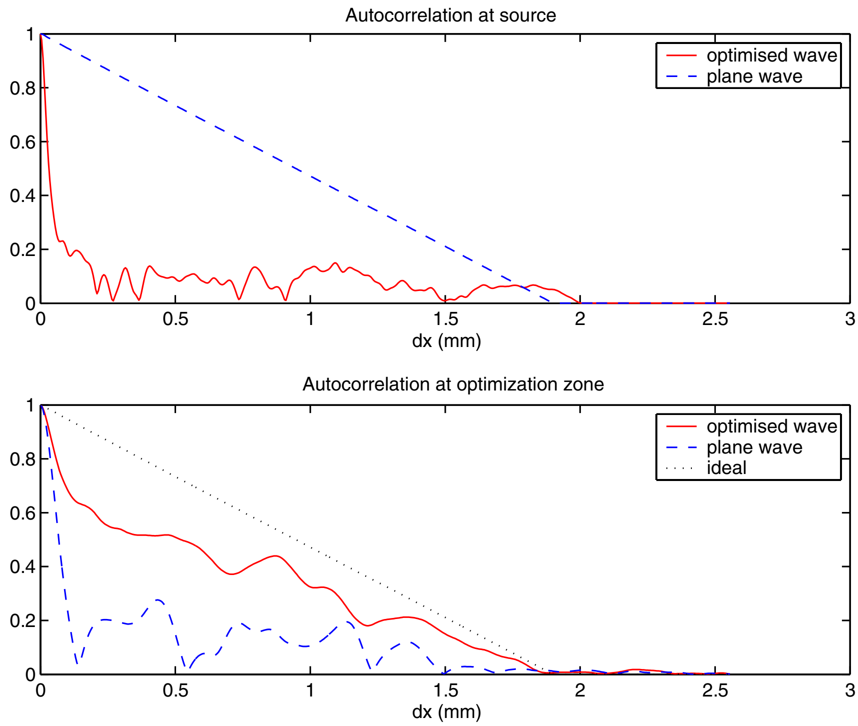

Fig. 7. Simulation of experiment showing increased spatial coherence at the measurement zone in the case of optimisation (top at source, bottom 5 mm from source).

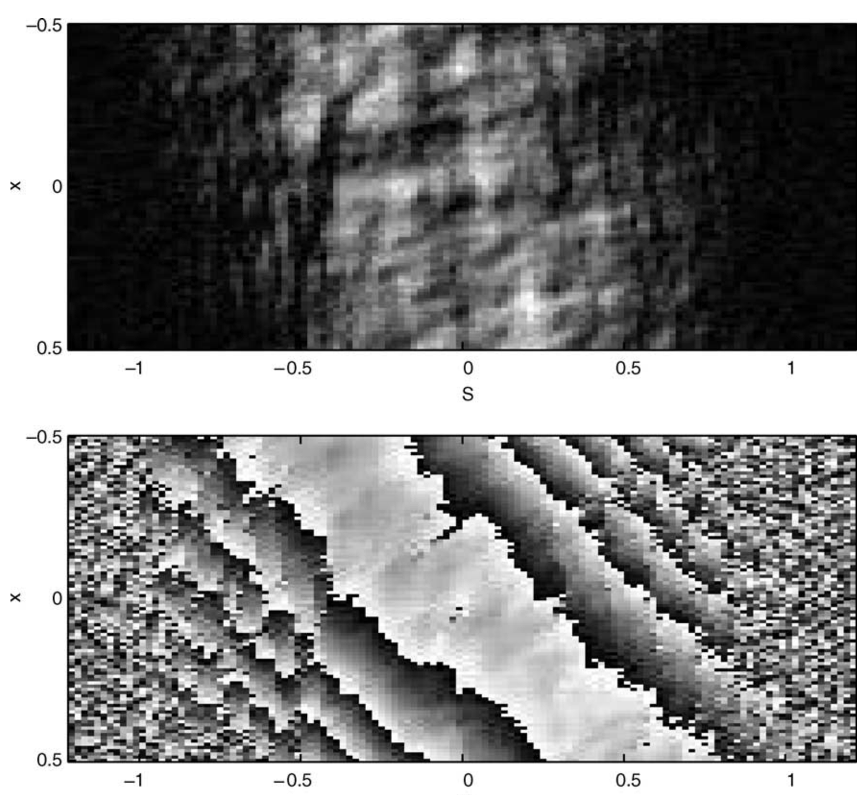

Fig. 8. A measured Green's function for a piece of steel (upper amplitude, lower phase). The axis labelled 'x' is the transverse receiver position (mm), the axis labelled 'S' is the source position (mm). The distance from the source to receiver was 8 mm.

Green's function was measured for a receiver patch 1 mm across, 2.5 mm deep at a mean distance of 7.75 mm from the source. The virtual source was scanned ±1.25 mm limited by the aperture of the spatial light modulator (SLM) in the OSAM. This data was then used to optimise the wavefront in the desired measurement area of 300 μm × 2.5 mm for a high, even amplitude and a flat wavefront. The resulting design phase ϕ_d was then used to program the SLM in the OSAM.

Fig. 9 shows the amplitude in the measurement zone taken using a flat (plane) wavefront and with an optimised wavefront. Fig. 9 also shows the velocity variation with position (assuming a 2 point velocity measurement technique [4]). Within the optimisation zone the

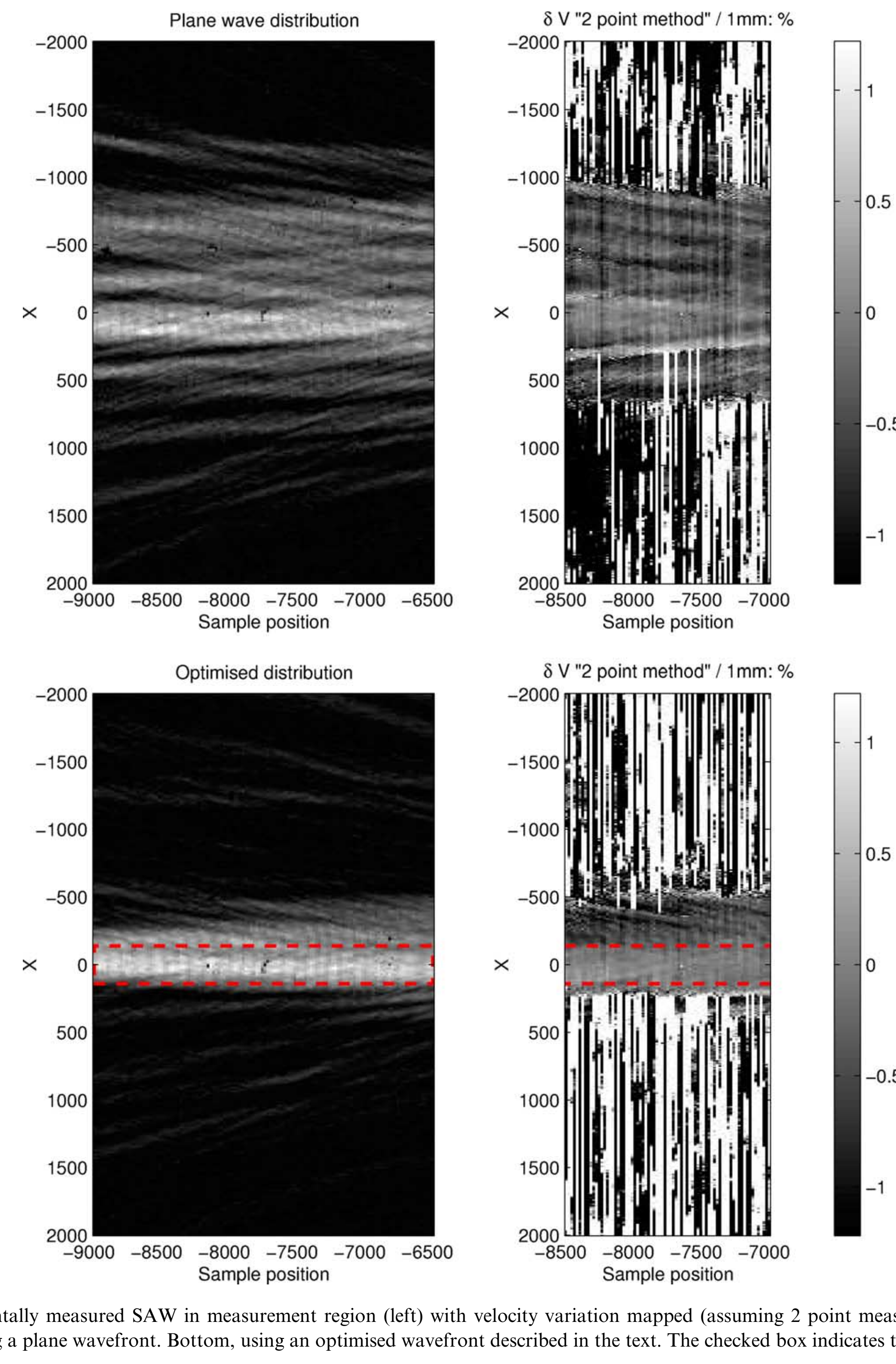

Fig. 9. Experimentally measured SAW in measurement region (left) with velocity variation mapped (assuming 2 point measurement over 1 mm) (right). Top, using a plane wavefront. Bottom, using an optimised wavefront described in the text. The checked box indicates the optimisation zone.

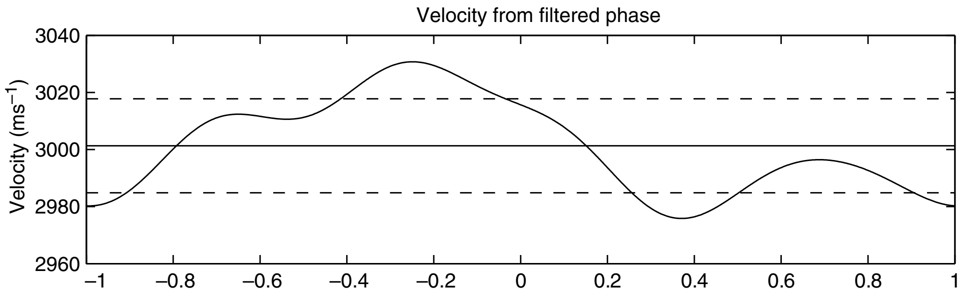

Fig. 10. Velocity measured via phase gradient technique using the optimised result in Fig. 9. A 200 μm averaging window has been used to reduce noise (primarily from the mechanical stages).

amplitude is high and even and the velocity variation (and hence the apparent velocity error) is lower than with the plane wavefront.

Using this optimised design it is possible to determine the velocity by looking the phase gradient (Fig. 10). The phase is determined by taking the phase of the zero-order of diffraction of the measurement region to avoid diffraction effects.

The variation of the velocity with distance (Fig. 10) is far greater than the expected experimental error ($<1/10^4$) and probably results from the varying sample of the microstructure. This error can be estimated from knowledge of the grain size as $\delta c \sim \frac{A\bar{c}}{\sqrt{(N)}} \sim \frac{0.25\times 3000}{\sqrt{2k}} \sim \pm 20$ ms^{-1}. where A is the degree of anisotropy, N is the number of grains sampled. In this case the grain size is $\sim$10 μm^3 and the sample size is 280 μm by $\sim$200 μm by $\sim$35 μm.

4. Conclusion

In this paper we have demonstrated the effect that aberrating materials can have on the acoustic wavefront and therefore on acoustic measurements. This can be severe acoustic speckle with large amplitude and phase fluctuations. We have also shown that the amplitude fluctuations caused by the acoustic speckle can be far more significant than attenuation caused by scattering.

An optimisation technique using measured Green's functions is demonstrated. This was designed to increase the spatial coherence and reduce error in a measurement zone away from the source. The measurement of the Green's function is necessary because it cannot be determined analytically without detailed prior knowledge of the sample microstructure.

Using a simulation environment the technique was shown to increase the spatial coherence *away* from the source as required.

Using an OSAM the technique was shown experimentally to reduce the variation in velocity measurement caused by acoustic aberrations. This is significant because it improves the measurement quality where simple adaption and correction or time reversal would struggle to make any improvement.

References

[1] S.D. Sharples, M. Clark, M.G. Somekh, All-optical adaptive scanning acoustic microscope, Ultrasonics 41 (4) (2003) 295–299.

[2] M. Clark, S.D. Sharples, M.G. Somekh, Laser ultrasonic microscopy, Material Evaluation 60 (9) (2002) 1094–1098.

[3] M. Clark, S.D. Sharples, M.G. Somekh, Fast all optical Rayleigh wave microscope: Imaging on isotropic and anisotropic materials, IEEE Transactions on Ultrasonics, Ferroelectrics and Frequency Control 47 (1) (1999) 65–74.

[4] M.G. Somekh, M. Liu, H.P. Ho, C.W. See, An accurate non-contacting laser based system for surface wave velocity measurement, Measurement Science and Technology 6 (1995) 1329–1337.

[5] S.D. Sharples, M. Clark, M.G. Somekh, Dynamic higher-order correction of acoustic aberration due to material microstructure, Appl. Phys. Lett. 81 (12) (2002) 2288–2290.

[6] S.D. Sharples, M. Clark, M. Somekh, Efficient and flexible laser ultrasound generation using spatial light modulators, Electronics Letters 37 (18) (2001) 1145–1146.

[7] M. Fink, Time reversal of ultrasonic fields—Parts I–III, IEEE Transactions on Ultrasonics, Ferroelectrics and Frequency Control 39 (5) (1992) 555–591.

[8] M. Clark, Two-dimensional, three-dimensional, and gray-scale images re-constructed from computer-generated holograms designed by use of a direct-search method, Applied Optics 38 (25) (1999) 5331–5337.

[9] J.W. Goodman, Introduction to Fourier Optics, McGraw-Hill, 1968.